Conditional filtering method for large-eddy simulation of turbulent nonpremixed combustion

Seung Hyun Kim[a] and Heinz Pitsch
Center for Turbulence Research, Stanford University, Stanford, California 94305-3035

(Received 8 December 2004; accepted 10 August 2005; published online 11 October 2005)

The conditional filtering method is proposed as a subfilter combustion model for large-eddy simulation (LES) of turbulent nonpremixed combustion. The novel method is based on conditional filtering of a reactive scalar field and an extension of conditional moment closure (CMC) for LES. Filtering conditioned on isosurfaces of the mixture fraction is adopted to resolve small-scale mixing and chemical reactions in nonpremixed combustion. The conditionally filtered equations are derived and the closure assumptions are discussed. *A priori* tests are performed using direct numerical simulation data for reacting mixing layers. The primary closure assumption on the subfilter flux in mixture fraction space is shown to work much better than the corresponding closure for the Reynolds averaged CMC due to resolved large-scale fluctuations of the scalar dissipation rate and of reactive scalars. Results show that first-order closure of the reaction rate performs well except for the boundaries of flame holes. In the boundaries of flame holes, fluctuations of reactive scalars around the conditionally filtered values are large enough for the effects of higher-order correlations to be significant. The accuracy of the first-order closure is less sensitive to the level of local extinction than that of first-order CMC, since large-scale fluctuations of reactive scalars on isosurfaces of the mixture fraction are resolved. This shows that extinction processes occur primarily over length scales comparable to the large scales of the turbulence. The integrated conditional filtering approach is introduced to reduce the computational cost and to resolve the low probability problem in the conditional filtering method. While the assumption of homogeneity in the integration direction is not as good as in the conditional average, the integrated formulation is shown to represent the extinction process caused by large-scale fluctuations of the scalar dissipation rate quite well. © *2005 American Institute of Physics*. [DOI: 10.1063/1.2084229]

I. INTRODUCTION

In the fast chemistry limit of turbulent nonpremixed combustion, turbulence does not affect the local flame structure and a reactive scalar is given as a function of the mixture fraction, which describes mixing of fuel and oxidizer.[1] This assumption allows the statistics of reactive scalars to be determined from those of the mixture fraction. Although the fast chemistry limit gives a leading-order solution for turbulent nonpremixed combustion, the separation of time scales is not generally acceptable due to a wide spectrum of time scales involved in turbulence and chemical reactions.

Turbulent straining enhances scalar gradients and diffusive heat loss from flames to surrounding fluid parcels. The scalar dissipation rate, which measures the diffusive mixing rate, is a critical parameter to describe nonequilibrium effects. With excessive scalar dissipation rate, nonpremixed flames may be locally extinguished. The extinguished flames may be reignited by diffusive transfer of heat and radicals from burning flames, when the scalar dissipation rate falls below a certain level. The modeling of local extinction and reignition requires a detailed description of the transient response of the local flame structure to scalar dissipation fluctuations.

[a]Author to whom correspondence should be addressed. Telephone: 650-723-9601. Fax: 650-725-3525. Electronic mail: shkcomb@stanford.edu

Large-eddy simulation (LES) offers two advantages over the Reynolds averaged Navier-Stokes (RANS) approach in computation of turbulent flames. First, mixing processes can be predicted with improved accuracy because large-scale structures dominating the global mixing characteristics are resolved in LES. Second, LES can capture the transient response of the local flame structure to the unsteadiness of the flow field on the order of the resolved time scale or longer. This makes LES attractive for the computation of turbulent flames, in which nonlinear interactions of turbulence and chemical reactions are of critical importance, e.g., for local extinction and reignition in turbulent nonpremixed flames.

Subfilter modeling of combustion processes in LES is a prominent research topic. Subfilter models often adopt the scale invariance assumption, which implies that certain features of physical processes are invariant at different length scales.[2] This assumption works well when the major part of subfilter contributions comes from length scales just smaller than the filter width. The scale invariance assumption is therefore not relevant to subfilter combustion processes, which mostly occur at the dissipative scales. The filtered density function method,[3] the linear eddy model,[4] the laminar flamelet model,[5] the conditional source term estimation,[6] and the flamelet/progress-variable approach[7] have been proposed as subfilter combustion models.

The conditional moment closure (CMC) model solves

the conditional moments of reactive scalars to resolve the closure problem of nonlinear chemical reactions.[8–10] In a turbulent nonpremixed flame, fluctuations of reactive scalars are primarily associated with those of the mixture fraction. Nonlinear chemical reactions can therefore be closed using statistics conditioned on the mixture fraction. The first-order CMC model, which assumes that fluctuations of the reactive scalars about the conditional means are small enough for chemical reactions to be closed using the conditional means, has been successfully applied to turbulent nonpremixed flames with low levels of local extinction.[11,12] Refined approaches, such as second-order closure and double conditioning, are being investigated for application to significant local extinction.[13–16] Although the CMC model has been extensively studied for RANS, there have been few studies in the context of LES.[6]

The objective of this study is to develop a subfilter combustion model for turbulent nonpremixed flames, based on the concept of CMC. In what follows, the conditionally filtered equations for reactive scalars are derived and closure assumptions are discussed. The integrated conditional filtering for a reacting shear layer is introduced. The closure assumptions and the performance of the model are tested with direct numerical simulation (DNS) data of reacting mixing layers.

II. MATHEMATICAL FORMULATION

A. Conditional filtering

Conventional filtering smooths out all small-scale details, and filtered chemical reaction rates are generally not well reconstructed from the (conventionally) filtered scalar field. In turbulent nonpremixed flames, the mixture fraction, which describes the extent of mixing of fuel and oxidizer, is a key quantity to describe the flame structure.[10] Here we adopt density-weighted filtering conditioned on isosurfaces of the mixture fraction to resolve small-scale mixing and chemical reactions in a nonpremixed flame,

$$\overline{\phi|\eta}(\eta,\mathbf{x},t) \equiv \frac{\int_V \rho\phi(\mathbf{x},t)\delta(\xi(\mathbf{x},t)-\eta)G(\mathbf{x}-\mathbf{x}';\Delta_f)d\mathbf{x}'}{\int_V \rho\delta(\xi(\mathbf{x},t)-\eta)G(\mathbf{x}-\mathbf{x}';\Delta_f)d\mathbf{x}'}, \tag{1}$$

where $G(\mathbf{x}-\mathbf{x}';\Delta_f)$ is a filtering function of specified width, Δ_f. We assume constant filter width so that the filtering operation commutes with differentiation. δ is the Dirac delta function and ξ is the mixture fraction. In Eq. (1), the filtering operates only on iso-η surfaces throughout because of the weighting with $\delta(\xi(\mathbf{x},t)-\eta)$. This decouples physical processes across a flame from those on a flame surface.

The filtered density function (FDF) and conditional mean density are, respectively, defined as[3]

$$P_\xi \equiv \int_V \delta(\xi(\mathbf{x},t)-\eta)G(\mathbf{x}-\mathbf{x}';\Delta_f)d\mathbf{x}', \tag{2}$$

$$\rho_\eta \equiv \frac{\int_V \rho\delta(\xi(\mathbf{x},t)-\eta)G(\mathbf{x}-\mathbf{x}';\Delta_f)d\mathbf{x}'}{P_\xi}. \tag{3}$$

The denominator of Eq. (1) is then given by $\rho_\eta P_\xi$. The density-weighted FDF is defined by

$$\bar{\rho}\widetilde{P}_\xi = \rho_\eta P_\xi, \tag{4}$$

where $\bar{\rho}$ is the filtered density. The density-weighted filtered value of ϕ can be calculated by integration in η space:

$$\widetilde{\phi} = \int_0^1 \overline{\phi|\eta}\widetilde{P}_\xi(\eta)d\eta. \tag{5}$$

The FDF can be modeled by a beta distribution in terms of the filtered value and subfilter variance of the mixture fraction.[17] While the FDF is stochastic and sometimes deviates from the Gaussian or beta distribution, the assumed beta distribution approach generally performs well for the mixture fraction.[17,18]

B. Conditionally filtered equation

The derivation of the unclosed equations for conditionally filtered reactive scalars is formally the same as that for conditionally averaged values.[10,19] Here, the derivation procedure is briefly described for completeness. The primary closure assumptions are then discussed.

The transport equation for the δ function[10] is given by

$$\frac{\partial\rho\delta_\eta}{\partial t} + \nabla\cdot(\rho\mathbf{v}\delta_\eta) = -\frac{\partial\delta_\eta\nabla\cdot(\rho D\nabla\xi)}{\partial\eta} = -\frac{\partial^2\rho\delta_\eta N}{\partial\eta^2} - \frac{\partial\nabla\cdot(\rho\delta_\eta D\nabla\xi)}{\partial\eta}, \tag{6}$$

where $\delta_\eta \equiv \delta(\xi(\mathbf{x},t)-\eta)$. D is the molecular diffusivity, which is assumed to be equal for all scalars here. $N \equiv D\nabla\xi\cdot\nabla\xi$ is the scalar dissipation rate. Filtering Eq. (6) gives

$$\frac{\partial\rho_\eta P_\xi}{\partial t} + \nabla\cdot(\rho_\eta\overline{\mathbf{v}|\eta}P_\xi) = -\frac{\partial\rho_\eta P_\xi\overline{M|\eta}}{\partial\eta}, \tag{7}$$

where $M \equiv 1/\rho\nabla\cdot(\rho D\nabla\xi)$ is the scalar diffusion rate. The relationship between $\overline{M|\eta}$ and $\overline{N|\eta}$ can be obtained using the identity in Eq. (6).

The conditionally filtered equation for a reactive scalar can be derived using the transport equation for the δ function. We have

$$\frac{\partial\nabla\cdot(\rho\delta_\eta D\nabla\xi)}{\partial\eta}Y_i = -\frac{\partial\rho\delta_\eta D\nabla\xi\cdot\nabla Y_i}{\partial\eta} + \frac{\partial\nabla\cdot(\rho\delta_\eta DY_i\nabla\xi)}{\partial\eta}, \tag{8}$$

$$\delta_\eta \nabla \cdot (\rho D \nabla Y_i) = \frac{\partial \rho \delta_\eta D \nabla \xi \cdot \nabla Y_i}{\partial \eta} + \nabla \cdot (\delta_\eta \rho D \nabla Y_i), \tag{9}$$

where Y_i is the mass fraction of species i. Using the above identities, we obtain

$$\begin{aligned}\frac{\partial \rho \delta_\eta Y_i}{\partial t} &+ \nabla \cdot (\rho \delta_\eta \mathbf{v} Y_i) \\ &= \rho \delta_\eta \omega_i - \frac{\partial^2 \rho \delta_\eta N Y_i}{\partial \eta^2} + 2\frac{\partial \rho \delta_\eta D \nabla \xi \cdot \nabla Y_i}{\partial \eta} \\ &- \frac{\partial \nabla \cdot (\rho \delta_\eta D Y_i \nabla \xi)}{\partial \eta} + \nabla \cdot (\delta_\eta \rho D \nabla Y_i),\end{aligned} \tag{10}$$

where ω_i is the chemical reaction rate of species i.

Filtering Eq. (10) gives

$$\begin{aligned}\frac{\partial \rho_\eta P_\xi \overline{Y_i|\eta}}{\partial t} &+ \nabla \cdot (\rho_\eta P_\xi \overline{\mathbf{v} Y_i|\eta}) \\ &= \rho_\eta P_\xi \overline{\omega_i|\eta} - \frac{\partial^2 \rho_\eta P_\xi \overline{N Y_i|\eta}}{\partial \eta^2} + 2\frac{\partial \rho_\eta P_\xi \overline{D \nabla \xi \cdot \nabla Y_i|\eta}}{\partial \eta} \\ &- \frac{\partial \nabla \cdot (\rho_\eta P_\xi \overline{Y_i D \nabla \xi|\eta})}{\partial \eta} + \nabla \cdot (\rho_\eta P_\xi \overline{D \nabla Y_i|\eta}).\end{aligned} \tag{11}$$

To identify the resolved part of the equation, we rewrite Eq. (11) as

$$\begin{aligned}\frac{\partial \rho_\eta P_\xi \overline{Y_i|\eta}}{\partial t} &+ \nabla \cdot (\rho_\eta P_\xi \overline{\mathbf{v}|\eta Y_i|\eta}) \\ &= \rho_\eta P_\xi \overline{\omega_i|\eta} + \frac{\partial \rho_\eta P_\xi R_i^\eta}{\partial \eta} + \rho_\eta P_\xi F_i + \rho_\eta P_\xi M_i,\end{aligned} \tag{12}$$

where

$$R_i^\eta \equiv \frac{1}{\rho_\eta P_\xi}\left[- \frac{\partial \rho_\eta P_\xi \overline{N|\eta Y_i|\eta}}{\partial \eta} + 2\rho_\eta P_\xi \overline{N|\eta} \frac{\partial \overline{Y_i|\eta}}{\partial \eta} \right], \tag{13}$$

$$F_i \equiv \frac{1}{\rho_\eta P_\xi}\left[- \nabla \cdot (\rho_\eta P_\xi J_i^{\mathbf{x}}) + \frac{\partial \rho_\eta P_\xi J_i^\eta}{\partial \eta} \right], \tag{14}$$

$$J_i^{\mathbf{x}} \equiv \overline{\mathbf{v} Y_i|\eta} - \overline{\mathbf{v}|\eta Y_i|\eta}, \tag{15}$$

$$J_i^\eta \equiv \frac{1}{\rho_\eta P_\xi}\left(- \frac{\partial \rho_\eta P_\xi \overline{N Y_i|\eta}}{\partial \eta} + 2\rho_\eta P_\xi \overline{D \nabla Y_i \cdot \nabla \xi|\eta} \right) - R_i^\eta, \tag{16}$$

$$\begin{aligned}M_i \equiv \frac{1}{\rho_\eta P_\xi}\Bigg[&- \frac{\partial \nabla \cdot (\rho_\eta P_\xi \overline{Y_i D \nabla \xi|\eta})}{\partial \eta} \\ &+ \nabla \cdot (\rho_\eta P_\xi \overline{D \nabla Y_i|\eta}) \Bigg].\end{aligned} \tag{17}$$

Here, the subfilter parts include correlations among subfilter fluctuations as well as those of filtered values and subfilter fluctuations. The conditionally filtered equations for other reactive scalars can be obtained by the same procedure.

$J_i^{\mathbf{x}}$ represents the subfilter scalar flux in $\mathbf{x}$ space. Since length scales for reignition fronts are not fully resolved in LES, $J_i^{\mathbf{x}}$ plays an important role in reignition of locally extinguished flames and stablization of lifted diffusion flames. Extinguished flames are reignited through transfer of heat and species from burning flames. Reignition may occur by edge flame propagation along isosurfaces of the mixture fraction and also by the engulfment mechanism involving diffusion normal to the iso-η surfaces.[20] In the conditionally filtered equation, transfer along the isopleth is described by the subfilter flux, $J_i^{\mathbf{x}}$, together with the molecular transport. Therefore, $J_i^{\mathbf{x}}$ is an important term to describe the premixed-type flame propagation along the isopleth. In the engulfment mechanism, flame folding by turbulent convection brings burning and extinguished flame elements closer to each other, and turbulent micromixing enhances heat and mass transfer by increasing surface area and local gradients. Reignition due to the engulfment mechanism thus involves diffusion normal to the isopleth as well as the circumferential diffusion. The diffusion normal to the isopleth is described by the second and third term on the right-hand side of Eq. (11).

The primary closure hypothesis of the conditional filtering method is concerned with J_i^η, which represents the effects of subfilter fluctuations of the scalar dissipation rate and the reactive scalars on the transport of the reactive scalars in η space. When we assume that reactive scalar fluctuations on the isosurfaces of the mixture fraction are primarily due to large-scale fluctuations of the scalar dissipation rate, the J_i^η term is expected to be much smaller than the resolved micromixing term, R_i^η, and we propose

$$F_i \approx - \frac{1}{\rho_\eta P_\xi} \nabla \cdot (\rho_\eta P_\xi J_i^{\mathbf{x}}). \tag{18}$$

Equation (18) is equivalent to the diffusion approximation of the reactive scalars in η space in CMC, which was validated against the DNS data.[13,15]

Next, we are concerned with the closure of M_i. It can be easily shown that

$$\begin{aligned}\nabla \cdot [\rho D \nabla (\delta_\eta Y_i)] = &- \frac{\partial \nabla \cdot (\rho \delta_\eta D Y_i \nabla \xi)}{\partial \eta} \\ &+ \nabla \cdot (\rho \delta_\eta D \nabla Y_i).\end{aligned} \tag{19}$$

When the density and the molecular diffusivity are constant, we have

$$\begin{aligned}\nabla \cdot [\rho D \nabla (P_\xi \overline{Y_i|\eta})] = &- \frac{\partial \nabla \cdot (\rho P_\xi D \overline{Y_i \nabla \xi|\eta})}{\partial \eta} \\ &+ \nabla \cdot (\rho D P_\xi \overline{\nabla Y_i|\eta}).\end{aligned} \tag{20}$$

The term M_i, therefore, represents the molecular transport of $\overline{Y_i|\eta}$ in $\mathbf{x}$ space. For RANS-based methods, the molecular transport is usually much smaller than the turbulent transport and neglected for high Reynolds number flows. However, in LES of turbulent combustion, the molecular transport term can be of the same order as the unresolved subfilter term. High temperature in the reaction zone gives much higher molecular transport coefficients than those of the cold mix-

ture, which can result in the relaminarization. Based on Eq. (20), we propose the following closure for M_i:

$$M_i \approx \frac{1}{\rho_\eta P_\xi} \nabla \cdot [\rho_\eta D_\eta \nabla (P_\xi \overline{Y_i|\eta})], \tag{21}$$

where $D_\eta \equiv \overline{D|\eta}$. Equation (21) is exact when ρ and D are constant.

C. Closure of chemical reaction rates

In turbulent nonpremixed flames, fluctuations of reactive scalars are primarily associated with those of the mixture fraction. However, fluctuations of reactive scalars on iso-η surfaces, which are much smaller than those in $\mathbf{x}$ space, can be significant when turbulent and chemical time scales are of the same order. Assuming that fluctuations on iso-η surfaces occur on the large scales, the conditionally filtered reaction rate can be calculated as

$$\overline{\omega_i(\rho,\mathbf{Y},T)|\eta} \approx \omega_i(\rho_\eta, \overline{\mathbf{Y}|\eta}, \overline{T|\eta}). \tag{22}$$

D. Integrated conditional filtering for a reacting shear layer

If the probability of finding a certain mixture fraction at a particular location becomes negligible, the conditionally filtered quantity may not be evaluated properly. For example, when we take measurements at the locations far from the axis of a turbulent jet diffusion flame, we seldom observe mixtures with $\xi \approx 1$, and the conditionally filtered quantities at $\eta \approx 1$ are not properly defined. The conditionally filtered equation is valid everywhere, but becomes trivial when P_ξ is negligible. It is physically meaningful in a small volume in the four-dimensional sample space, $(\mathbf{x}, \eta)$, where P_ξ is not negligible. Here, integrated conditional filtering is introduced as an alternative for Eq. (1), which is computationally less expensive and solves this low probability problem. An integrated conditionally filtered function is defined as

$$\overline{\phi|\eta}^*(\eta,x_2,x_3,t) \equiv \frac{\int_{-\infty}^{\infty} w \int_V \rho\phi(\mathbf{x},t)\delta(\xi(\mathbf{x},t)-\eta)G(\mathbf{x}-\mathbf{x}';\Delta_f)d\mathbf{x}'dx_1}{\int_{-\infty}^{\infty} w \int_V \rho\delta(\xi(\mathbf{x},t)-\eta)G(\mathbf{x}-\mathbf{x}';\Delta_f)d\mathbf{x}'dx_1}, \tag{23}$$

where w is a weighting factor that depends on the coordinate system. The integration direction depends on the case, but should go through the flame brush and should be aligned as closely as possible with the gradient of the mixture fraction. In a round jet flame $x_1 = w = r$, where r is the radial coordinate. Alternatively, a nonisotropic filter, for which a filter scale for the x_1 direction is much larger than that for the x_2 and x_3 directions, can be used. The integrated FDF and conditional mean density are, respectively, defined as

$$P_\xi^* = \int_{-\infty}^{\infty} w \int_V \delta(\xi(\mathbf{x},t)-\eta)G(\mathbf{x}-\mathbf{x}';\Delta_f)d\mathbf{x}'dx_1, \tag{24}$$

$$\rho_\eta^* \equiv \frac{\int_{-\infty}^{\infty} w \int_V \rho\delta(\xi(\mathbf{x},t)-\eta)G(\mathbf{x}-\mathbf{x}';\Delta_f)d\mathbf{x}'dx_1}{P_\xi^*}. \tag{25}$$

The denominator of Eq. (23) is then given by $\rho_\eta^* P_\xi^*$.

The equation for $\overline{Y_i|\eta}^*$ can be written as

$$\frac{\partial \rho_\eta^* P_\xi^* \overline{Y_i|\eta}^*}{\partial t} + \nabla_\perp \cdot (\rho_\eta^* P_\xi^* \overline{\mathbf{v}|\eta}^* \overline{Y_i|\eta}^*) = \rho_\eta^* P_\xi^* \overline{\omega_i|\eta}^* + \frac{\partial \rho_\eta^* P_\xi^* R_i^{\eta *}}{\partial \eta} + \rho_\eta^* P_\xi^* F_i^* + \rho_\eta^* P_\xi^* M_i^*, \tag{26}$$

where

$$R_i^{\eta *} \equiv \frac{1}{\rho_\eta^* P_\xi^*}\left[- \frac{\partial \rho_\eta^* P_\xi^* \overline{N|\eta}^* \overline{Y_i|\eta}^*}{\partial \eta} + 2\rho_\eta^* P_\xi^* \overline{N|\eta}^* \frac{\partial \overline{Y_i|\eta}^*}{\partial \eta}\right], \tag{27}$$

$$F_i^* \equiv \frac{1}{\rho_\eta^* P_\xi^*}\left[- \nabla_\perp \cdot (\rho_\eta^* P_\xi^* J_i^{\mathbf{x}*}) + \frac{\partial \rho_\eta^* P_\xi^* J_i^{\eta *}}{\partial \eta}\right], \tag{28}$$

$$J_i^{\mathbf{x}*} \equiv \overline{\mathbf{v}Y_i|\eta}^* - \overline{\mathbf{v}|\eta}^* \overline{Y_i|\eta}^*, \tag{29}$$

$$J_i^{\eta *} \equiv \frac{1}{\rho_\eta^* P_\xi^*}\left[- \frac{\partial \rho_\eta^* P_\xi^* \overline{NY_i|\eta}^*}{\partial \eta} + 2\rho_\eta^* P_\xi^* \overline{D \nabla Y_i \cdot \nabla \xi|\eta}^*\right] - R_i^{\eta *}. \tag{30}$$

The superscript $*$ represents the integrated quantity. $\nabla_\perp$ is a two-dimensional gradient operator. This is the conservative form of the conditionally filtered species equation. The nonconservative form can be obtained using the equation for P_ξ^*:

$$\frac{\partial \rho_\eta^* P_\xi^*}{\partial t} + \nabla_\perp \cdot (\rho_\eta^* \overline{\mathbf{v}|\eta}^* P_\xi^*) = - \frac{\partial \rho_\eta^* P_\xi^* \overline{M|\eta}^*}{\partial \eta}. \tag{31}$$

Subtracting Eq. (31) multiplied by $\overline{Y_i|\eta}^*$ from Eq. (26) gives

$$\frac{\partial \overline{Y_i|\eta}^*}{\partial t} + \overline{\mathbf{v}|\eta}^* \cdot \nabla_\perp \overline{Y_i|\eta}^* = \overline{N|\eta}^* \frac{\partial^2 \overline{Y_i|\eta}^*}{\partial \eta^2} + \overline{\omega_i|\eta}^* + F_i^* + \nabla_\perp \cdot (D_\eta^* \nabla_\perp \overline{Y_i|\eta}^*), \tag{32}$$

where the term involving the gradient of P_ξ^* multiplied by D_η^* is assumed to be negligible compared with the other terms. This equation has a similar form to the Eulerian laminar flamelet model of Pitsch.[5] In this derivation, the laminar flamelet equations, which are originally in a Lagrangian-like coordinate system, have been transformed to an Eulerian system, which introduces spatial dependence and convective transport terms. It was then argued that changes in the flame structure mainly occur in downstream and azimuthal directions. Variations of the flame structure in radial direction have therefore been neglected. The instantaneous velocity and scalar dissipation rate were replaced by the filtered values to apply these equations as a subfilter combustion model. Here a rigorous derivation is presented with the exact definition of the conditionally filtered quantities used in the integrated approach. More importantly, Eq. (32) includes the subfilter transport term, F_i^*, and the molecular transport term,

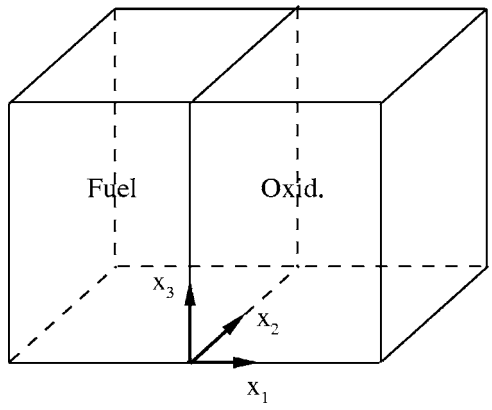

FIG. 1. Schematic of the computational domain.

which are neglected in the Eulerian flamelet model. Closure of F_i^* will be addressed in a subsequent section.

III. DIRECT NUMERICAL SIMULATION

DNS was performed to validate the present formulation. Figure 1 shows a schematic of the computation domain. The simulated flow field is a shear-free, temporally developing mixing layer. Initially separated fuel and oxidizer mix in the presence of decaying turbulence, and react according to a single-step reaction,

$$\mathrm{F} + \mathrm{O} \rightarrow 2\mathrm{P}$$

where F, O, and P represent fuel, oxidant, and product, respectively. The stoichiometric mixture fraction is 0.5 and the reaction rate is given by

$$\omega = A\rho Y_F Y_O \exp\left(-\frac{\beta}{(1+\alpha\theta)}\right), \tag{33}$$

where Y_F and Y_O represent the mass fractions of fuel and of oxidizer, respectively. $\theta \equiv (T-T_0)/(T_f-T_0)$ is the nondimensional temperature, where T_f and T_0 represent the adiabatic flame temperature and reference temperature, respectively. The heat release parameter, $\alpha \equiv T_f/T_0 - 1$, is given by $q/(c_p T_0)$, where q and c_p are heat release per unit mass and the specific heat at constant pressure, respectively. $\beta \equiv T_a/T_0$ is the nondimensional activation temperature, where T_a is the activation temperature. Chemical parameters used here are $\alpha=6$ and $\beta=28$. The preexponential factor A is adjusted to control the level of local extinction.

The fully compressible Navier-Stokes equations are solved with the conservation equations of the mass fractions of the fuel and the oxidizer. A low-storage fourth-order Runge-Kutta method is used for time integration, while spatial derivatives are evaluated with a sixth-order compact finite-difference scheme.[21,22] The computation domain is periodic in the x_2 and x_3 directions, while it has nonreflecting boundaries in the x_1 direction.[23] Table I shows characteristics of the simulations. The initial Mach number based on the rms velocity fluctuations and the temperature of fuel and oxidizer is below 0.1 for all the cases, so that compressibility effects are negligible. The dynamic viscosity is constant for the given case here. The case C2 is the reference case. The level of local extinction for C3 is lower than that for C2, while that for C1 is more significant. The cases C4 and C5 have a higher Reynolds number than the other cases and assume constant density. For these cases, the nondimensional temperature θ is set to be the product mass fraction.

IV. RESULTS AND DISCUSSION

Figure 2 shows the instantaneous fields of the product mass fraction on an x_1-x_2 plane for the higher Reynolds number case C5 at $\tau \approx 1.5$, where the nondimensional time τ is normalized by the initial eddy turn over time. There is significant local extinction in Fig. 2. The extinguished part of the flame surface is of large scale and is not much distorted by small-scale eddies, indicating that extinction processes are dominated by large-scale structures in this case. The product concentration is high near a vortex core where the scalar dissipation is low. Note that the variation of Y_P along the stoichiometric surface is significant near the vortex core. Rolling up of the flame surface around the vortex core brings extinguished and burning flames closer to each other.

Figure 3 shows the average scalar fluxes for the nondimensional temperature, θ, in mixture fraction space at $\tau \approx 1.5$ for C5. A top hat filter with a filter width of $\Delta_f = 8\Delta$ was used, where Δ is the grid spacing in DNS. The average of the resolved flux, R_θ^η, is in good agreement with the total flux, $R_\theta^\eta + J_\theta^\eta$. This justifies the primary closure assumption, Eq. (18). The corresponding closure for the Reynolds averaged CMC overpredicts the scalar flux in mixture fraction space.

The accuracy of the closure assumption, Eq. (18), can be measured by the average of $\overline{NY_i|\eta_{\mathrm{st}}} - \overline{N|\eta_{\mathrm{st}}Y_i|\eta_{\mathrm{st}}}/\overline{N|\eta_{\mathrm{st}}Y_i|\eta_{\mathrm{st}}}$, where $\cdot|\eta_{\mathrm{st}}$ denotes the filtered quantity on the stoichiometric surface. The closure assumption works better when the absolute value of this quantity becomes smaller. For the case C5, the average of $\overline{N\theta|\eta_{\mathrm{st}}} - \overline{N|\eta_{\mathrm{st}}\theta|\eta_{\mathrm{st}}}/\overline{N|\eta_{\mathrm{st}}\theta|\eta_{\mathrm{st}}}$ is -0.06, while the corresponding

TABLE I. Characteristics of the simulations (l: integral length scale, l_K: Kolmogorov length scale; u': rms velocity; Δ: grid spacing; Re_λ: Taylor scale Reynolds number; $\mathrm{Da} \equiv A\rho_0 l/u'$; ρ_0: reference density).

Case	Da	q	l/u'	l/l_K	Δ/l_K	Re_λ	Grid
C1	2.52E+4	$\alpha c_p T_0$	1.03	27.1	1.37	47	$192\times128\times128$
C2	7.57E+4	$\alpha c_p T_0$	1.03	27.1	1.37	47	$192\times128\times128$
C3	1.51E+5	$\alpha c_p T_0$	1.03	27.1	1.37	47	$192\times128\times128$
C4	2.0E+3	0	0.80	50.2	1.72	73.5	$256\times256\times256$
C5	4.0E+3	0	0.80	50.2	1.72	73.5	$256\times256\times256$

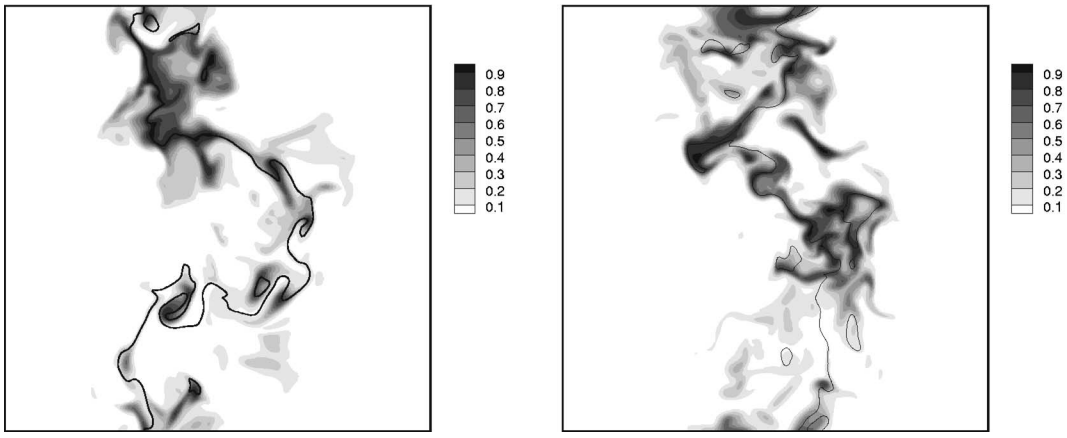

FIG. 2. Instantaneous fields of the product mass fraction on two x_1-x_2 planes for C5 (the line represents the stoichiometric surface).

value for the Reynolds averaged CMC is −0.39. Therefore, the effects of subfilter fluctuations of the scalar dissipation rate and the reactive scalars in the present method are much smaller than those for the Reynolds averaged CMC. The closure assumption works better for the conditional filtering method, since large-scale fluctuations of the scalar dissipation rate and the reactive scalars are resolved.

The underlying assumption of the conditional filtering method is that fluctuations of reactive scalars on isosurfaces of the mixture fraction are primarily due to large-scale fluctuations of the scalar dissipation rate. The justification of this assumption has been discussed in Pitsch.[5] For a further validation, we need to investigate the length scales of scalar dissipation fluctuations on iso-η surfaces. Figure 4 shows the distribution of the scalar dissipation rate in an x_2-x_3 plane for the higher Reynolds number case C5 at $\tau \approx 1.5$. High scalar dissipation rates are associated with thin sheetlike structures in Fig. 4. The length scales of scalar dissipation rate across flames are much smaller than those along flame surfaces. Figure 5 shows the distribution of the integrated scalar dissipation rates on the stoichiometric surfaces, N^*_{st}, for C5. Scalar dissipation rates for $0.4<\xi<0.6$ are averaged in the x_1 direction. Note that the structures with high scalar dissipation rates have a range of length scales, and that higher scalar dissipation rates are associated with large-scale structures. The structures with $N^*_{\mathrm{st}}>5\langle N|\eta_{\mathrm{st}}\rangle$ have the size of $0.4<l<0.8$ in Fig. 5, where l and $\langle N|\eta_{\mathrm{st}}\rangle$ are the integral length scale and the conditional mean scalar dissipation rate at the stoichiometric mixture fraction, respectively.

Figure 6 shows the probability density function (PDF) of the ratio of the filtered root mean square fluctuations of the conditional scalar dissipation rate to the corresponding filtered mean, $\gamma \equiv \sqrt{\overline{N''^2|\eta_{\mathrm{st}}}}/\overline{N|\eta_{\mathrm{st}}}$, for the case C5. A top hat filter with a filter width of $\Delta_f=8\Delta$ was used. When low scalar dissipation events are taken with the condition of $\overline{N|\eta_{\mathrm{st}}}<\langle N|\eta_{\mathrm{st}}\rangle$ small-scale fluctuations of the conditional scalar dissipation rate are significant. Note that the PDF of γ for high scalar dissipation events is significantly different from that for low scalar dissipation events. The PDF for high scalar dissipation events with the condition of $\overline{N|\eta_{\mathrm{st}}}>5\langle N|\eta_{\mathrm{st}}\rangle$

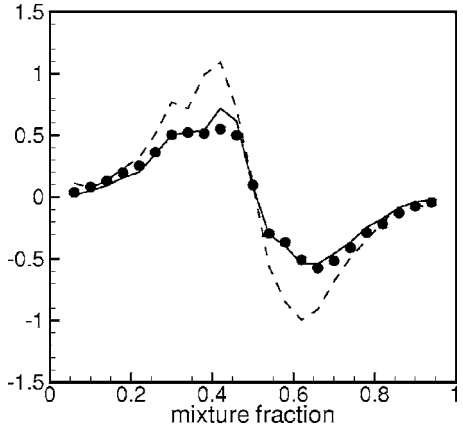

FIG. 3. Average scalar fluxes in mixture fraction space for C5 (symbols: total flux $R^{\eta}_{\theta}+J^{\eta}_{\theta}$, solid line: resolved flux R^{η}_{θ}, dashed line: scalar flux in the Reynolds averaged CMC; the quantities are normalized by the product of the conditional averages of the nondimensional temperature θ and the scalar dissipation rate N at the stoichiometric mixture fraction; $\Delta_f/\Delta=8$).

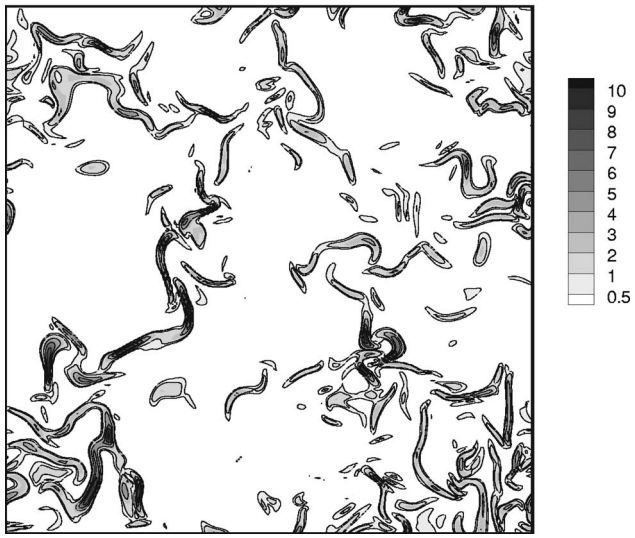

FIG. 4. Distribution of the scalar dissipation rate on x_2-x_3 plane for C5 ($x_1=0$; the scalar dissipation rate is normalized by the conditional mean scalar dissipation rate at the stoichiometric mixture fraction).

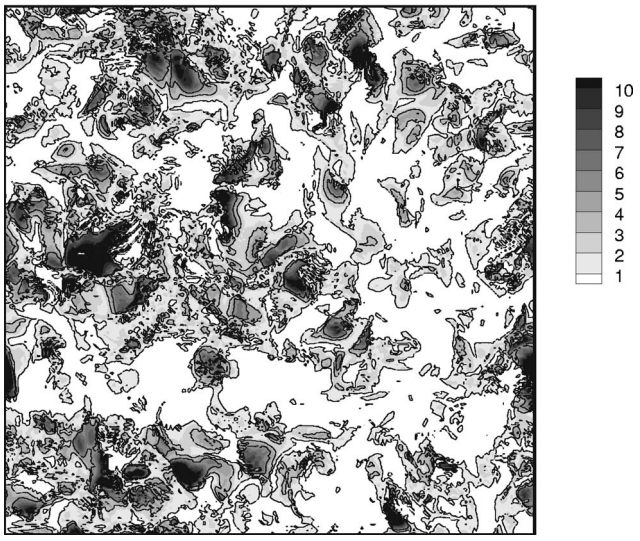

FIG. 5. Distribution of the scalar dissipation rate averaged in the x_1 direction with the condition of $0.4<\xi<0.6$ for C5 (the scalar dissipation rate is normalized by the conditional mean scalar dissipation rate at the stoichiometric mixture fraction).

has a sharp peak at $\gamma_\eta \approx 0.17$. Most of the probability is confined in $\gamma_\eta < 0.5$ when $\overline{N|\eta_{st}} > 3\langle N|\eta_{st}\rangle$.

Figure 7 shows the PDFs of the normalized scalar dissipation rate at the stoichiometric mixture fraction $\chi \equiv N_{st}/\langle N|\eta_{st}\rangle$ and the corresponding filtered value $\bar{\chi} \equiv \overline{N|\eta_{st}}/\langle N|\eta_{st}\rangle$ for the case C5. Apparently, the filtered value represents the PDF fairly well, except for very small values of the dissipation rate. As in Fig. 6, small-scale fluctuations of the conditional scalar dissipation rate are of relative importance in low scalar dissipation region, while these fluctuations are much smaller than fluctuations in large scales. Filtering in the low scalar dissipation region thus reduces the probability of finding very low scalar dissipation. The underprediction of the PDF of very low scalar dissipation events is, however, of minor importance in prediction of the flame structure, since the local flame structure for low scalar dissipation rates is close to chemical equilibrium. Note that the conditionally filtered scalar dissipation captures most of high scalar dissipation events in Fig. 7. The PDF of $\bar{\chi}$ closely follows that of χ for $0.2<\bar{\chi}<15$, while the maximum of χ in the flow field is about 20. Although the filtered scalar dissipation does not capture extremely high scalar dissipation events, the probability of finding $\chi>15$ is very small.

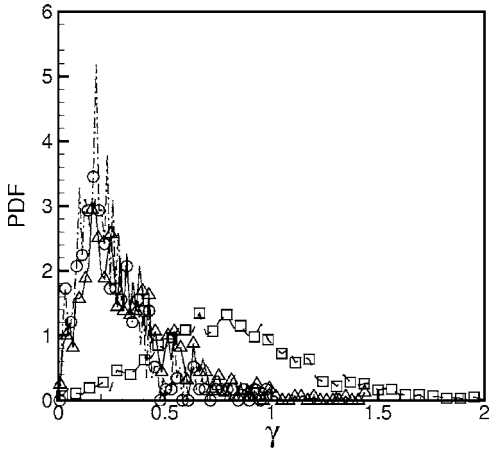

FIG. 6. Probability density function of the ratio of the filtered root mean square fluctuations of the conditional scalar dissipation rate to the corresponding filtered mean for C5 ($\gamma \equiv \sqrt{\overline{N'^2|\eta_{st}}}/\overline{N|\eta_{st}}$, square: low scalar dissipation events with $\overline{N|\eta_{st}} < \langle N|\eta_{st}\rangle$, delta: $\overline{N|\eta_{st}} > 3\langle N|\eta_{st}\rangle$, circle: $\overline{N|\eta_{st}} > 5\langle N|\eta_{st}\rangle$, where $\langle N|\eta_{st}\rangle$ is the conditional mean scalar dissipation rate at the stoichiometric mixture fraction and $\Delta_f/\Delta=8$).

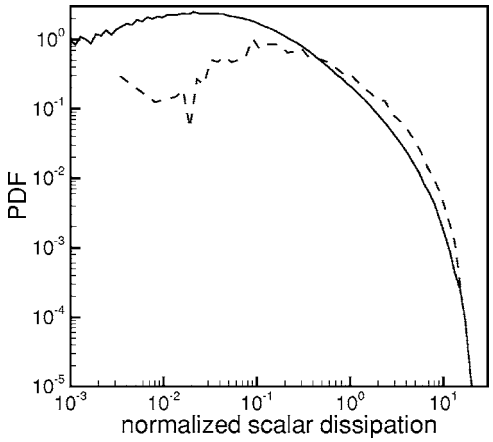

FIG. 7. Probability density functions of the normalized scalar dissipation rate at the stoichiometric mixture fraction and the corresponding filtered value for C5 (solid line: $\chi=N_{st}/\langle N|\eta_{st}\rangle$, dashed line: $\bar{\chi}=\overline{N|\eta_{st}}/\langle N|\eta_{st}\rangle$, where $\langle N|\eta_{st}\rangle$ is the conditional mean scalar dissipation rate at the stoichiometric mixture fraction and $\Delta_f/\Delta=8$).

When the compressive strain generated by counterflow-like, large-scale velocity structures is aligned with the mean scalar gradient, sharp fronts of the scalar are formed.[24,25] The length of the fronts is on the order of an integral scale, while the thickness of this front is manifested at small scales.[25] These sheet-like structures are known to be associated with the ramp-cliff structures and indicative of direct interaction of small and large scales. These structures are also observed at relatively high Reynolds numbers. As the Reynolds number increases, the thickness of the layer decreases, giving higher scalar dissipation values.[26]

Nonpremixed flames are sensitive to the spatial and temporal fluctuations of the scalar dissipation rate. With excessive scalar dissipation rate, nonpremixed flames may be locally extinguished and flame holes appear. Since extinction occurs in high scalar dissipation regions, cliffs in the ramp-cliff structure are a primary source of local extinction events. Considering scalar dissipation fluctuations conditioned on the isoscalar surfaces, the variations across the layer are suppressed. The variations of high values of the conditional scalar dissipation then occur on large scales along the sheet-like structures, which constitute the cliffs. Small-scale fluctuations of the conditional scalar dissipation rate along the sheet-like structures are usually much smaller than the difference of the conditional scalar dissipation in and out of the sheet-like structures. As pointed out by Warhaft,[25] larger velocity structures are likely to generate steeper scalar gradients.

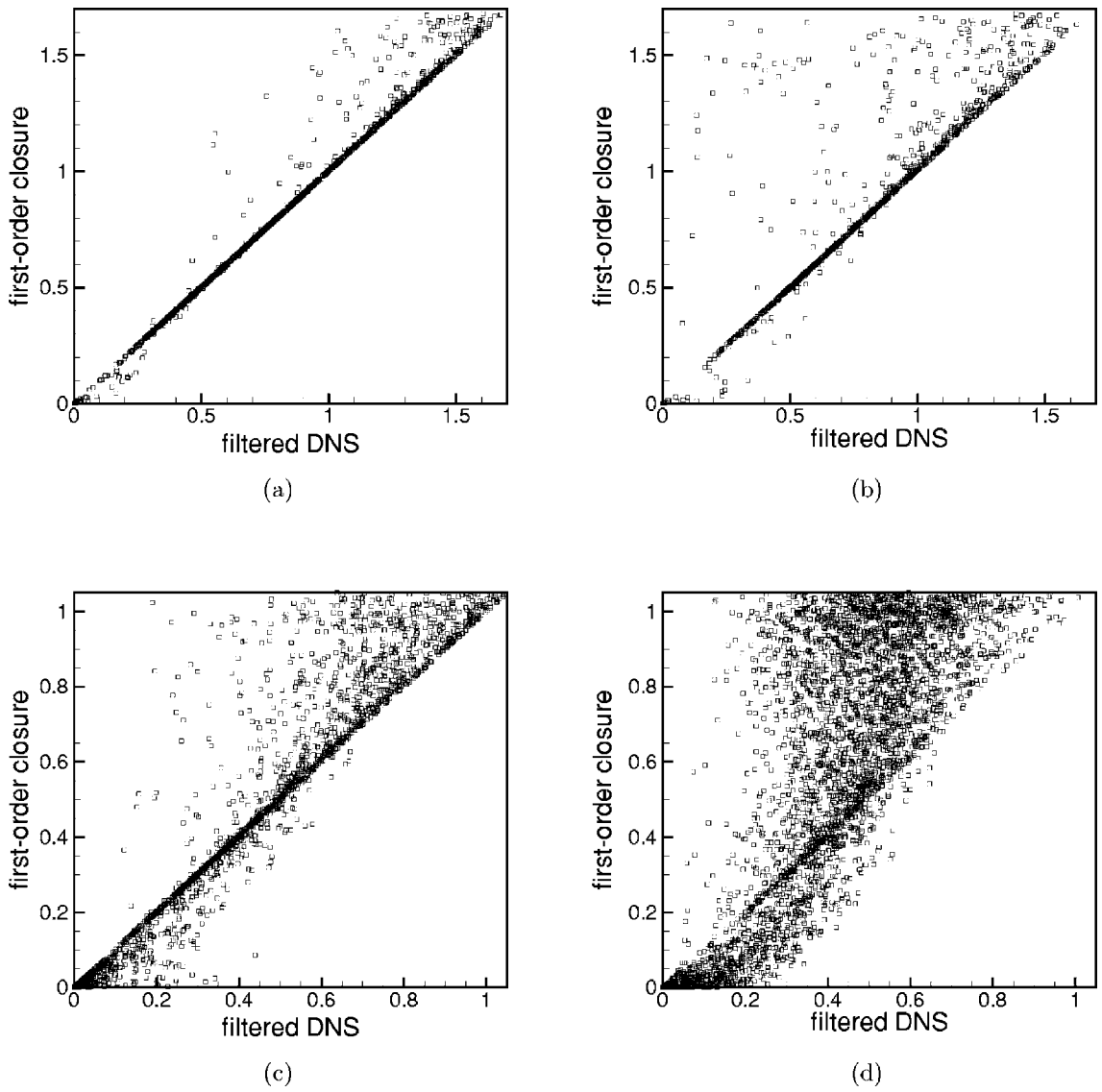

FIG. 8. Correlation for conditionally filtered reaction rates at the stoichiometric mixture fraction (a) $\overline{\omega|\eta_{st}}$ for C2, (b) $\overline{\omega|\eta_{st}}^*$ for C2, (c) $\overline{\omega|\eta_{st}}$ for C5, and (d) $\overline{\omega|\eta_{st}}^*$ for C5 ($\Delta_f/\Delta=8$).

Figure 8(a) shows the conditionally filtered reaction rates, $\omega|\eta_{st}$, for the reference case C2 at $\tau\approx 2.0$. A filter width of $\Delta_f=8\Delta$ was used. The predicted reaction rates are in excellent agreement with the filtered DNS data in Fig. 8(a), while they are slightly overpredicted for a small fraction of points with higher reaction rates. The first-order closure tends to overpredict the reaction rates when the reactive scalars fluctuate near the maximum reaction rate. The overprediction of the reaction rates occurs in the region close to interface between burning and extinguished flames. In that region, the conditional subfilter fluctuations of reactive scalars are large enough for the higher-order correlations to be non-negligible. Figure 8(b) shows the integrated reaction rate, $\overline{\omega|\eta_{st}}^*$, for C2. The overall agreement is similar to that for $\omega|\eta_{st}$. Figure 8(c) shows the conditionally filtered reaction rates, $\omega|\eta_{st}$, for the higher Reynolds number case C5 at $\tau\approx 1.5$. The prediction is well correlated with the filtered DNS, while it is more scattered than in C2. Here, in addition to the overprediction at higher reaction rates, the reaction rates are underpredicted at lower values. The first-order closure tends to underpredict the reaction rates when the reactive scalars fluctuate near the minimum reaction rate. In Fig. 8(d), the accuracy of the integrated reaction rate for C5 is not good due to unresolved scalar fluctuations in the integration direction. The normalized error for the predicted reaction rates is defined as[17]

$$\epsilon=\left[\frac{\sum(\overline{\omega|\eta_{st}}-\omega(\overline{\mathbf{Y}|\eta_{st}},\overline{T|\eta_{st}}))^2}{\sum\overline{\omega|\eta_{st}}^2}\right]^{1/2}. \tag{34}$$

The error for the data presented in Fig. 8 is less than 0.3 except for those for Fig. 8(d). The error for all test cases is given in Tables II and III.

In a turbulent shear layer, the variation of the conditional Reynolds average in the transverse direction is quite small.[27] *A priori* tests show that the variation of the conditionally filtered quantity is not as small as that of the conditional average. As shown in Fig. 2, due to the folding of the flame

TABLE II. Normalized error for $\overline{\omega|\eta_{st}}$.

Δ_f/Δ	4	8	12	16	32
C1	0.020	0.068	0.121	0.175	0.344
C2	0.027	0.076	0.138	0.191	0.387
C3	0.031	0.073	0.137	0.155	0.316
C4	0.063	0.175	0.255	0.316	0.493
C5	0.096	0.246	0.362	0.459	0.709

TABLE III. Normalized error for $\overline{\omega|\eta_{st}}^*$.

Δ_f/Δ	4	8	12	16	32
C1	0.158	0.224	0.284	0.343	0.514
C2	0.167	0.295	0.323	0.400	0.594
C3	0.095	0.187	0.246	0.299	0.375
C4	0.371	0.451	0.493	0.521	0.551
C5	0.511	0.660	0.743	0.832	1.01

surface, burning and extinguished flame elements can coexist in the integration direction. The averages have then contributions from the flames with different strain rate histories, which causes errors in the integrated approach. The variation of the conditional average is not significant because flame surfaces fluctuate in the shear layer.

To compare the performance of the model to the Reynolds averaged first-order CMC, the conditional mean reaction rates for the reference case C2 and the higher Reynolds number case C5 are shown in Fig. 9. Conditional means and conditionally filtered values of reactive scalars are taken from the DNS data. The first-order CMC significantly overpredicts the reaction rate for both cases. The predictions are much improved if Δ_f/Δ is less than 16. As Δ_f/Δ increases, the subfilter fluctuations become more significant and the predictions approach the first-order CMC results. The overprediction of the reaction rate is more significant for C5.

Conditional filtering adds a new independent variable in the system of equations, which substantially increases the computational cost. However, the computational cost can be reduced when the characteristics of the conditionally filtered equations are properly considered. $P_\xi(\eta_{st})$ has a very narrow distribution as compared with the thickness of the mixing layer, as shown in Fig. 2. Since all the terms in the conservative form of the conditionally filtered equations are weighted by P_ξ, only a small region of $(\mathbf{x},\eta)$ space is *active*. Hence, the equations do not need to be solved in regions where P_ξ is negligible. A moving grid technique can be used to reduce the memory requirement for the conditionally filtered equations. With a moving grid, often only a few grid points are needed to resolve variations of the conditionally filtered reactive scalars in the x_1 direction. Another way to reduce the computational cost is the integrated conditional filtering approach. In this approach, the number of independent variables is reduced by one due to integration in one spatial coordinate.

Figure 10 shows the distribution of P_ξ^* near $(x_2,x_3)=(0,0)$ for C5. The integrated FDF P_ξ^* represents mixing characteristics averaged over the x_1 direction, the behavior of which is quite different from the FDF P_ξ. P_ξ^* has similar shape to the PDF of the mixture fraction in this flow configuration. In Fig. 10, P_ξ^* has spikes at $\eta=0$ and 1, which indicate the presence of fresh fuel and oxidant. While P_ξ significantly varies along the x_1 direction, the integrated FDF P_ξ^* has a weak spatial dependence in Fig. 10.

Figure 11 shows the behavior of $\overline{N|\eta}^*$ for C5. Here, $\overline{N|\eta}^*$ is normalized by $\langle N|\eta_{st}\rangle$. The variations of $\overline{N|\eta}^*$ are significant both in the shape and in the magnitude. The predictions by the following model are also presented in Fig. 11:

$$\overline{N|\eta}^* = \frac{\int_{-\infty}^{\infty} \rho_\eta P_\xi N_0 \exp\{-2[\mathrm{erf}^{-1}(2\eta-1)]^2\}dx_1}{\int_{-\infty}^{\infty} \rho_\eta P_\xi dx_1}, \tag{35}$$

where

$$N_0 = \frac{\tilde{N}}{\int_0^1 \exp\{-2[\mathrm{erf}^{-1}(2\eta-1)]^2\}\tilde{P}_\xi(\eta)d\eta}. \tag{36}$$

The filtered scalar dissipation $\tilde{N}$ and the FDF are taken from the DNS. Note that the model predictions follow the charac-

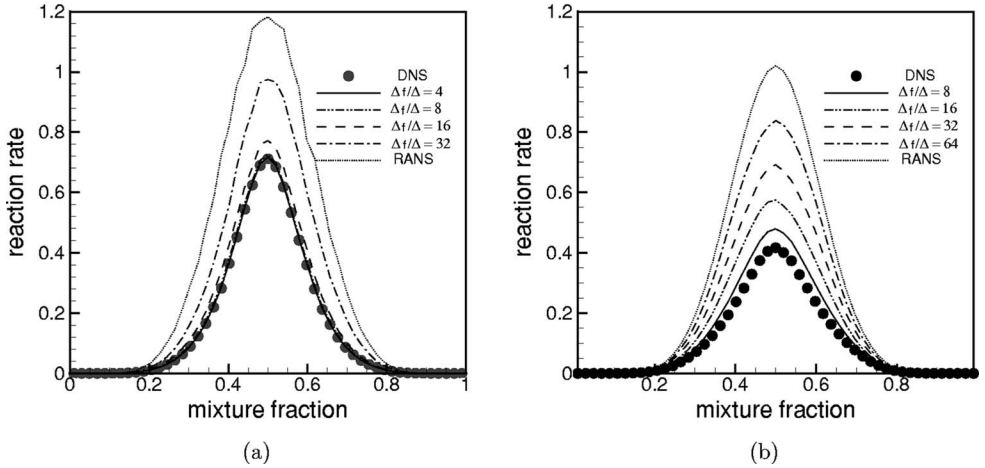

FIG. 9. Conditional mean reaction rates (a) C2, (b) C5.

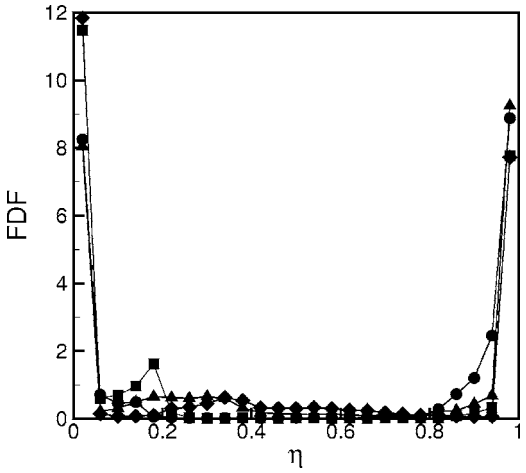

FIG. 10. Integrated filtered density function P_ξ^* at several locations near $(x_2,x_3)=(0,0)$ for C5 ($\tau\approx 1.5$).

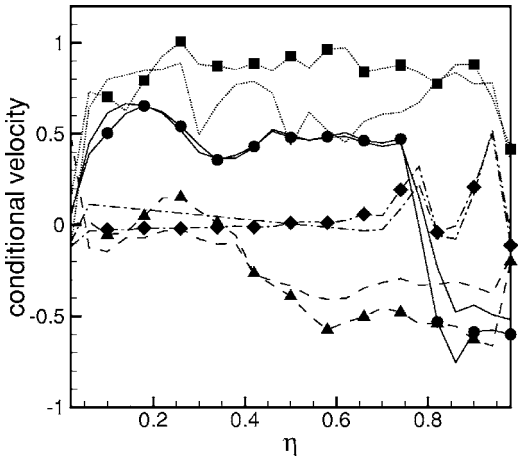

FIG. 12. Conditionally filtered velocity $\overline{v_2|\eta_{st}}^*$ at several locations for C5 (symbols: DNS, lines: model, $\tau\approx 1.5$).

teristic of $\overline{N|\eta}^*$ well. The base function in Eq. (35) is obtained by the amplitude mapping closure and follows a scalar dissipation profile in the laminar counterflow configuration.[28] The local mixing characteristics are considered by the FDF weighted integral in Eq. (35).

Figure 12 shows the behavior of $\overline{v_2|\eta}^*$ for C5. The predictions by the following model are compared with the DNS data:

$$\overline{v_i|\eta}^* = \frac{\int_{-\infty}^{\infty} \rho_\eta P_\xi \overline{v_i|\eta} dx_1}{\int_{-\infty}^{\infty} \rho_\eta P_\xi dx_1}, \tag{37}$$

where

$$\overline{v_i|\eta} = \tilde{v}_i + \frac{\widetilde{v_i\xi} - \tilde{v}_i\tilde{\xi}}{\sigma_\xi^2}(\eta - \tilde{\xi}). \tag{38}$$

σ_ξ^2 and v_i are the subfilter variance of the mixture fraction and the velocity component in the x_i direction, respectively. The filtered values for the mixing field are taken form the DNS. Equation (38) is exact when the mixture fraction and velocity are Gaussian.[29] Equation (37) performs well for the present case.

The integrated conditional filtering equation, Eq. (32), is solved to validate the performance of the model. $\overline{N|\eta}^*$ and $\overline{\mathbf{v}|\eta}^*$ are taken from the DNS data to avoid ambiguity in the modeling of the flow and mixing field. The conditional subfilter scale flux, $J_i^{\mathbf{x}*}$, is modeled by an eddy diffusivity model,

$$J_i^{\mathbf{x}*} \approx -D_t \nabla \overline{Y_i|\eta}^*, \tag{39}$$

where D_t is given by

$$D_t = c_q \Delta_f^2 \sqrt{2\bar{S}_{ij}^* \bar{S}_{ij}^*}. \tag{40}$$

$\bar{S}_{ij}$ is the filtered strain rate tensor. Although a dynamic model could be used to determine the value of c_q, a constant value of $c_q=0.1$ has been used here. While the flux is formulated for the values averaged over the x_1 direction, the filter width in the transport directions, x_2 and x_3, is Δ_f. Because $\rho_\eta^* P_\xi^*$ has a weak spatial dependence, F_i^* can be approximated as

$$F_i^* \approx \nabla \cdot (D_t \nabla \overline{Y_i|\eta}^*). \tag{41}$$

The filter width is taken as $\Delta_f = 8\Delta$. The physical domain is discretized into 32×32 grid points, while 50 grid points are used in mixture fraction space.

The spatial distributions of $\overline{Y_P|\eta_{st}}^*$ at $\tau\approx 1.5$ for C5 and at $\tau\approx 2.0$ for C1 are shown in Fig. 13. The present method predicts the location and size of flame holes for C1 with good accuracy. Flame holes with large length scales are also well predicted for the higher Reynolds number case C2.

The present method resolves the effects of large-scale fluctuations of the conditional scalar dissipation rate on the local flame structure. The importance of large-scale fluctua-

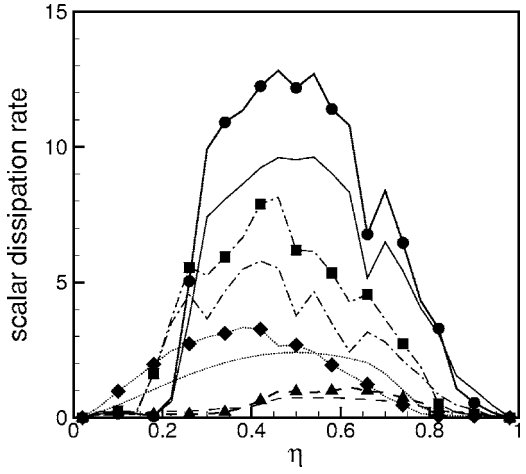

FIG. 11. Conditionally filtered scalar dissipation rate $\overline{N|\eta_{st}}^*$ at several locations for C5 (symbols: DNS, lines: model, $\overline{N|\eta_{st}}^*$ is normalized by the conditional mean scalar dissipation at the stoichiometric mixture fraction $\langle N|\eta_{st}\rangle$, $\tau\approx 1.5$).

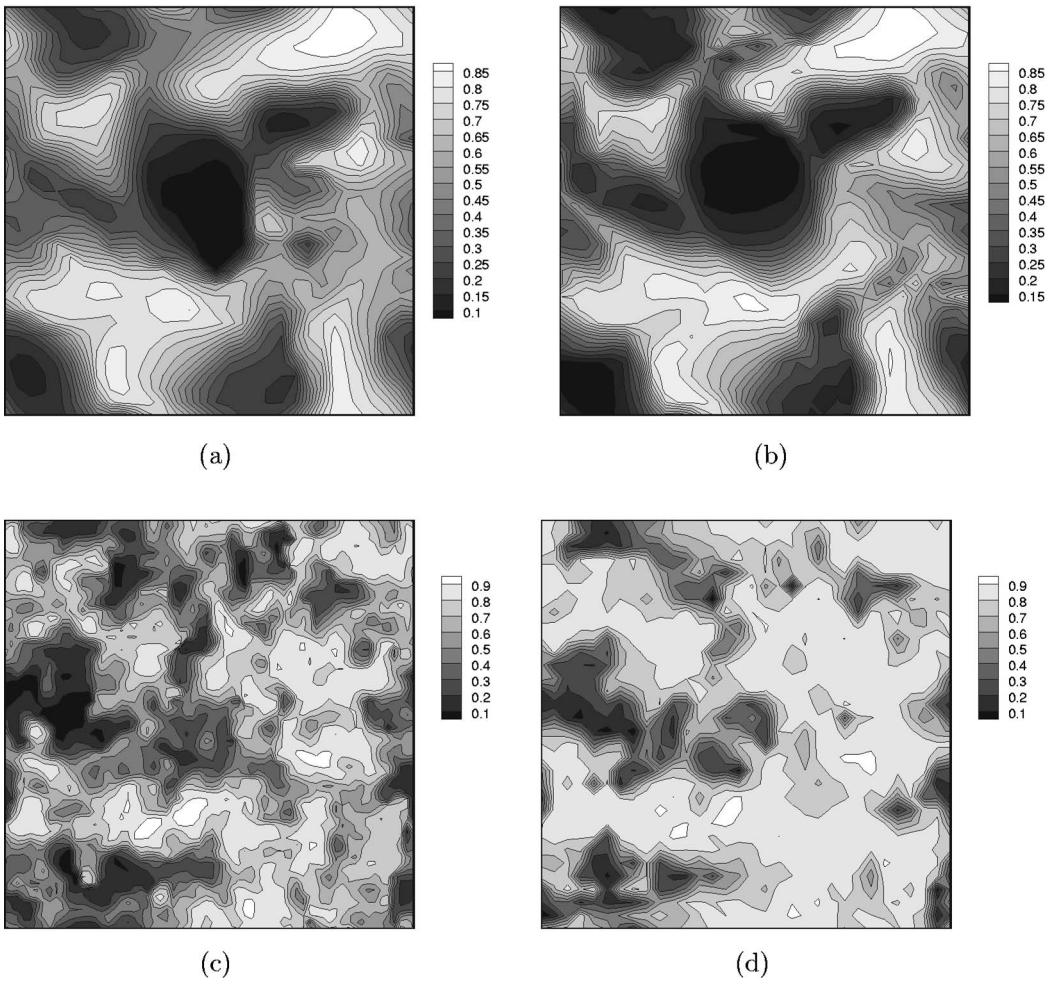

FIG. 13. Distribution of conditionally filtered mass fraction of product at the stoichiometric mixture fraction: (a) filtered DNS data for C1, (b) conditional filtering method for C1, (c) filtered DNS data for C5, and (d) conditional filtering method for C5.

tions of the scalar dissipation rate in CMC was first pointed out by Klimenko.[30] He argued that large-scale fluctuations of the scalar dissipation rate are of importance in generation of conditional fluctuations of reactive scalars. Pitsch[5] showed in LES of a turbulent methane/air jet flame that the prediction of pollutant formation can be improved by considering large-scale fluctuations of the scalar dissipation rate. Independent of the present work, Navarro-Martinez *et al.*[31] presented a CMC-based subfilter combustion model and applied it to the same flame as that studied in Pitsch.[5] They also obtained an improved prediction of intermediate species and NO with consideration of large-scale scalar dissipation fluctuations.

Since high scalar dissipation events are associated with the large-scale velocity structures, the size of the flame holes is expected to be primarily of large scale, which is shown in Fig. 13. This is also supported by the experimental data.[32,33] Schefer[32] presented flame sheet imaging using CH chemiluminescence in turbulent jet diffusion flames. In the experimental image, flame holes are primarily of large scale. It was also observed that the length scale of flame holes increases downstream. Hult *et al.*[33] reported a detailed experimental study of local extinction in the "DLR_B" turbulent jet diffusion flame. In analysis of time-resolved measurements of OH, temperature, and velocity fields, they pointed out that most of the extinction events are associated with large-scale flow structures.

While the present method resolves the global variations in burning and extinguished flames, which primarily occur on large scales, it does not resolve fluctuations associated with the edge flame propagation. First-order closure of conditionally filtered reaction rates, therefore, is inaccurate on the boundaries of flame holes. Unresolved scalar dissipation fluctuations may result in underprediction of large excursion of reactive scalars. Second-order closure can be used to consider the unresolved reactive scalar fluctuations.[10,13,14]

V. CONCLUSIONS

The conditional filtering method is proposed as a subfilter model for LES of turbulent nonpremixed combustion. Filtering on isosurfaces of the mixture fraction is adopted to resolve small-scale mixing and chemical reactions in nonpremixed combustion. The conditionally filtered equations are derived and *a priori* tests are performed to validate the closure assumptions and the model performance.

In the conditional filtering method, reactive scalar fluctuations induced by large-scale scalar dissipation fluctuations on isosurfaces of the mixture fraction can be considered in the first-order closure level in the present cases. The primary closure assumption on the subfilter flux in mixture fraction space works much better than the corresponding closure for the Reynolds averaged CMC due to resolved large-scale conditional fluctuations of the scalar dissipation rate and of reactive scalars. First-order closure of the reaction rate performs well everywhere, except for the boundaries of flame holes. In the boundaries of flame holes, fluctuations of reactive scalars around the conditionally filtered values are large enough for the effects of higher-order correlations to be significant. The effects of the subfilter fluctuations become more important as the filter width and the area of flame hole boundaries increase. The accuracy of the first-order closure is less sensitive to the level of local extinction than that of first-order CMC for RANS, since large-scale fluctuations of reactive scalars on isosurfaces of the mixture fraction are resolved.

The integrated conditional filtering approach is introduced to reduce the dimensionality of the problem and to resolve the low probability problem in the conditional filtering method. With significant level of local extinction, the integrated formulation is found to give additional errors in the conditionally filtered reaction rate due to unresolved scalar fluctuations in the integration direction. Higher-order closure is needed to consider these unresolved scalar fluctuations. However, the integrated formulation is shown to represent extinction processes caused by large-scale fluctuations of the scalar dissipation rate quite well.

[1] R. W. Bilger, *Turbulent Reacting Flows*, edited by P. A. Libby and F. A. Williams (Springer, Berlin, 1980), pp. 65–113.
[2] C. Meneveau and J. Katz, "Scale-invariance and turbulence models for large eddy simulation," Annu. Rev. Fluid Mech. **32**, 1 (2000).
[3] F. A. Jaberi, P. J. Colucci, S. James, P. Givi, and S. B. Pope, "Filtered mass density function for large-eddy simulation of turbulent reacting flows," J. Fluid Mech. **401**, 85 (1999).
[4] A. R. Kerstein, "Linear eddy model of turbulent transport, Part 7. Finite rate chemistry and multi stream mixing," J. Fluid Mech. **240**, 289 (1992).
[5] H. Pitsch, "Improved pollutant predictions in large-eddy simulation of turbulent nonpremixed combustion by considering scalar dissipation fluctuations," Proc. Combust. Inst. **29**, 1971 (2002).
[6] W. K. Bushe and H. Steiner, "Conditional moment closure for large eddy simulation of nonpremixed turbulent reacting flows," Phys. Fluids **11**, 1896 (1999).
[7] C. D. Pierce and P. Moin, "Progress-variable approach for large-eddy simulation of non-premixed turbulent combustion," J. Fluid Mech. **504**, 73 (2004).
[8] R. W. Bilger, "Conditional moment closure for turbulent reacting flow," Phys. Fluids A **5**, 436 (1993).
[9] A. Y. Klimenko, "Multicomponent diffusion of various admixtures in turbulent flow," Fluid Dyn. **25**, 327 (1990).
[10] A. Y. Klimenko and R. W. Bilger, "Conditional moment closure for turbulent combustion," Prog. Energy Combust. Sci. **25**, 595 (1999).
[11] S. H. Kim, K. Y. Huh, and T. Liu, "Application of the elliptic conditional moment closure model to a two-dimensional nonpremixed methanol bluff-body flame," Combust. Flame **120**, 75 (2000).
[12] N. S. A. Smith, R. W. Bilger, C. D. Carter, R. S. Barlow, and J. Y. Chen, "A comparison of CMC and PDF modelling predictions with experimental nitric oxide LIF/Raman measurements in a turbulent H_2 jet flame," Combust. Sci. Technol. **105**, 357 (1995).
[13] S. H. Kim, K. Y. Huh, and R. W. Bilger, "Second-order conditional moment closure modelling of local extinction and reignition in turbulent nonpremixed hydrocarbon flames," Proc. Combust. Inst. **29**, 2131 (2002).
[14] S. H. Kim and K. Y. Huh, "Second-order conditional moment closure modelling of turbulent piloted jet diffusion flames," Combust. Flame **138**, 336 (2004).
[15] A. Kronenberg, "Double conditioning of reactive scalar transport equations in turbulent nonpremixed flames," Phys. Fluids **16**, 2640 (2004).
[16] C. M. Cha and H. Pitsch, "Higher-order conditional moment closure modelling of local extinction and reignition in turbulent combustion," Combust. Theory Modell. **6**, 425 (2002).
[17] C. Wall, B. J. Boersma, and P. Moin, "An evaluation of the assumed beta probability density function subgrid-scale model for large eddy simulation of nonpremixed turbulent combustion with heat release," Phys. Fluids **12**, 2522 (2000).
[18] C. Tong, "Measurements of conserved scalar filtered density function in a turbulent jet," Phys. Fluids **13**, 2923 (2001).
[19] S. H. Kim, "On the conditional variance and covariance equations for second-order conditional moment closure," Phys. Fluids **14**, 2011 (2002).
[20] P. Sripakagorn, S. Mitarai, G. Kosaly, and H. Pitsch, "Extinction and reignition in a diffusion flame: A direct numerical study," J. Fluid Mech. **518**, 231 (2004).
[21] C. A. Kennedy, M. H. Carpenter, and R. M. Lewis, "Low-storage, explicit Runge-Kutta schemes for the compressible Navier-Stokes equations," Appl. Numer. Math. **35**, 177 (2000).
[22] S. K. Lele, "Compact finite difference schemes with spectral-like resolution," J. Comput. Phys. **103**, 16 (1992).
[23] T. J. Poinsot and S. K. Lele, "Boundary conditions for direct numerical simulations of compressible viscous flows," J. Comput. Phys. **101**, 104 (1992).
[24] B. I. Shriman and E. D. Siggia, "Scalar turbulence," Nature (London) **405**, 639 (2000).
[25] Z. Warhaft, "Passive scalars in turbulent flows," Annu. Rev. Fluid Mech. **32**, 203 (2000).
[26] C. Tong and Z. Warhaft, "On passive scalar derivative statistics in grid turbulence," Phys. Fluids **6**, 2165 (1994).
[27] A. Y. Klimenko, "Note on the conditional moment closure in turbulent shear flows," Phys. Fluids **7**, 446 (1995).
[28] E. E. O'Brien and T. L. Jiang, "The conditional dissipation rate of an initially binary scalar in homogeneous turbulence," Phys. Fluids A **3**, 3121 (1991).
[29] V. R. Kuznetsov and V. A. Sabel'nikov, *Turbulence and Combustion*, English edition, edited by P. A. Libby (Hemisphere, New York, 1990).
[30] A. Y. Klimenko, "Conditional moment closure and large scale fluctuations of scalar dissipation," Fluid Dyn. **28**, 630 (1993).
[31] S. Navarro-Martinez, A. Kronenberg, and F. D. Mare, "Conditional moment closure for large eddy simulations," Flow, Turbul. Combust. (to be published).
[32] R. W. Schefer, "Flame sheet imaging using CH chemiluminescence," Combust. Sci. Technol. **126**, 255 (1997).
[33] J. Hult, U. Meier, W. Meier, A. Harvey, and C. F. Kaminski, "Experimental analysis of local flame extinction in a turbulent jet diffusion flame by high repetition 2D laser techniques and multi-scalar measurements," Proc. Combust. Inst. **30**, 701 (2005).